International Journal of Medical Physics, Clinical Engineering and Radiation Oncology, 2022, 11, 125-134
https://www.scirp.org/journal/ijmpcero
ISSN Online: 2168-5444
ISSN Print: 2168-5436

Image Quality Assessment Using NEMA Standards for Lu-177 Radionuclide

Olivia Adu-Poku[1,2*], Bright Kwakye-Awuah[1], Eric Kotei Addison[1,2], Stephen Inkoom[3,4]

[1]Department of Physics, Kwame Nkrumah University of Science and Technology, Kumasi, Ghana
[2]Komfo Anokye Teaching Hospital, Oncology Directorate, Department of Medical Physics, Kumasi, Ghana
[3]Department of Medical Physics, Graduate School of Nuclear and Allied Sciences, University of Ghana, Accra, Ghana
[4]Radiation Protection Institute, Ghana Atomic Energy Commission, Accra, Ghana
Email: *oadu-poku@knust.edu.gh, missolive70@ymail.com

How to cite this paper: Adu-Poku, O., Kwakye-Awuah, B., Addison, E.K. and Inkoom, S. (2022) Image Quality Assessment Using NEMA Standards for Lu-177 Radionuclide. *International Journal of Medical Physics, Clinical Engineering and Radiation Oncology*, **11**, 125-134.
https://doi.org/10.4236/ijmpcero.2022.113011

Received: April 13, 2022
Accepted: July 1, 2022
Published: July 4, 2022

Abstract

A lutetium 177 (^{177}Lu) radiopharmaceutical has been used as a theragnostic agent in molecular radiotherapies. This study aimed to produce images simulating those obtained in a total body imaging study with hot lesions to assess and investigate the image quality of the Hawkeye SPECT/CT images from Lu-177. The NEMA image quality phantom (PTW) with spheres (inner diameters of 10, 13, 17, 22, 28 and 37 mm) and lung insert was used. The measured volume in the background of the current phantom setting was 9482 mL. The five smaller spheres were filled with an activity concentration of 0.461 MBq/mL and the biggest sphere was filled with water. The phantom was placed on the couch and scanned at four hot sphere-to-background concentrations, which are no background, 16:1, 8:1 and 4:1. The images obtained from the scans were imported onto the OXIRIS image analysis tool. Regions of interest (ROIs) were drawn on each sphere of the reconstructed SPECT image. Image contrast and background variability ratios for hot spheres were used as measures of image quality. In addition, the accuracy of corrections were determined from the uniform background and cold lung insert regions. The 37 mm cold sphere had the highest percent contrast, whiles the 10 mm hot sphere had the least for the various hot sphere to background ratios. The background variability for each hot sphere was also determined. The average lung residual error was calculated to be 23.13% for the 16:1 and 22.57% for both the 8:1 and 4:1 hot sphere to background ratio. The results show that the scanner has very good overall performance.

Keywords

Lutetium-177, Activity Concentration, Dose Calibrator, SPECT/CT

1. Introduction

The radioactive lutetium 177 (^{177}Lu) has been found to be useful in a variety of applications for radionuclide therapy tumor treatment. Due to its favourable decay characteristics, which have not only β-particle emissions with the maximum energy of 498.3 keV, but are also associated with two peaks of γ-ray emission with the energies of 112.9 and 208.4 keV, ^{177}Lu has been widely used as the theragnostic agent to provide the diagnostic and therapeutic procedures in radionuclide therapy [1]. MIRD Report No. 26 [1] has issued a guideline for quantitative ^{177}Lu SPECT for dosimetry and radiopharmaceutical therapy. The imaging system can estimate the absorbed dose for ^{177}Lu quantification using either a planar or tomographic gamma camera imaging. SPECT tomographic imaging enables more precise image quantification as well as absorbed dose estimation as compared to planar imaging. [2] [3]. The image quality of a system, on the other hand, could have a substantial impact on SPECT image quantification. The performance of imaging modalities in diagnostic medical imaging must be examined and assessed on a regular basis to maintain proper functionality and image quality. A variety of methodologies are used to analyze systems [4] [5]. The National Electrical Manufacturers Association (NEMA) has established a standard for evaluating the performance of SPECT scanners [3]. When introducing a new system or evaluating the quality of a given SPECT system over time, such image quality control measurements are also required in SPECT/CT hybrid imaging for SPECT performance measurements [4] [5]. NEMA IQ phantom measurements are also used in clinical investigations comparing SPECT/CT and SPECT/MR imaging performance in patients [6] [7]. Furthermore, investigations studying the attenuating influence of new hardware components developed for use in PET/MR systems, such as radiofrequency (RF) coils [8] [9] and radiotherapy planning equipment [10] require accurate NEMA IQ phantom measurements. NEMA IQ phantom measurements have also been used in dose optimization experiments for PET/MR hybrid imaging [11]. All of these research are based on precise methods for attenuation correction (AC) of the phantoms in question. The obtained SPECT data must be corrected for photon attenuation induced by the scanned object as well as the attenuating hardware components of the system in order to obtain quantitative SPECT images that can be used to estimate scanner performance characteristics [12]. This study investigates the standard NEMA image quality test using CT-based AC for the SPECT/CT hybrid system. Contrast recovery, background variability and signal-to-noise ratio are determined. In comparison, the effect of CT-based AC is evaluated and the impact on the image quality parameters is assessed.

2. Materials and Method

2.1. Radionuclide Calibrator

All activities prepared were measured using the IBC NM dose calibrator. Lu-177 vials were put at the bottom of a syringe holder raised at 3 cm relative to its normal

position in order to place the vials closer to the area of the highest sensitivity.

2.2. NEMA Image Quality-Recovery Coefficients

The NEMA image quality phantom (PTW) with spheres of inner diameters 10, 13, 17, 22, 28 and 37 mm plus a lung insert were used for this test. Four syringes were first prepared to fill the phantom with four different hot-sphere to background ratios as shown in Table 1. The measured volume in the background of the current phantom setting was 9482 ml. The largest sphere was filled with water to estimate errors due to scattering. A lung insert was mounted (as shown in Figure 1) to estimate scatter and attenuation correction errors. The remaining five spheres were filled with activity concentrations of 0.461 MBq/ml prepared in a syringe. The phantom positioned on the couch as shown in Figure 2 and was initially scanned with no background activity. Another activity concentration of 288.05 MBq was prepared and disbursed into the phantom background and was scanned at 16:1 hot-sphere-to background ratio. Same procedure was repeated for 8:1 and 4:1 hot-sphere to background ratios. The prepared activities with four different hot-sphere to background ratios are shown in Table 1 below. Figure 3 shows the CT and SPECT images from NEMA image quality test for no background, 4:1, 8:1 and 16:1 hot sphere-to-background ratios.

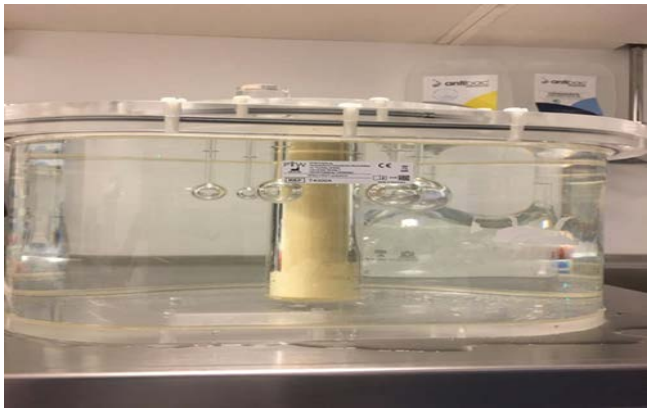

Figure 1. The NEMA IEC body phantom with six spheres and a lung insert.

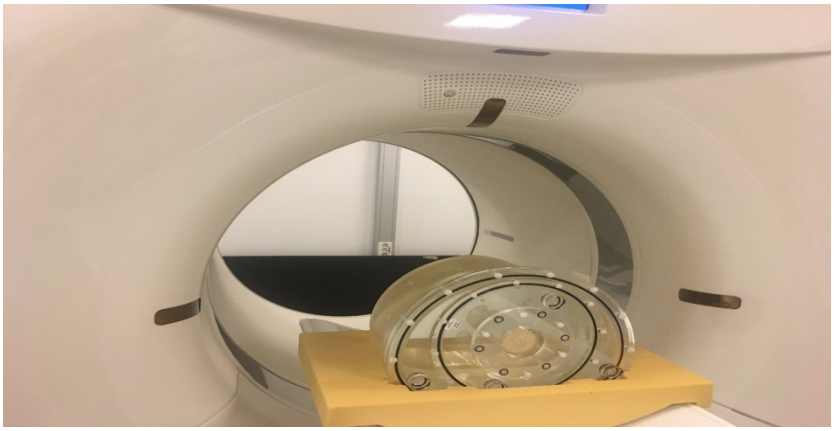

Figure 2. Image quality test acquisition.

Table 1. NEMA phantom preparation. Four syringes prepared to fill the phantom with four different hot sphere to background ratios.

	Prepared Activity [MBq]	Residual Activity [MBq]	Total Activity [MBq]	Diluted volume [mL]	Activity concentration [kBq/mL]	Actual hot sphere to background ratio
Syringe 1 Spheres	50.6	4.5	46.1	100	461	No background
Syringe 2 Background (16:1)	297	8.95	288.05	9482	30.38	15.2:1
Syringe 3 Background (8:1)	294	10.70	283.3 + 288.05 = 571.35	9482	60.26	7.65:1
Syringe 4 Background (4:1)	635.5	0	635.5 + 571.35 = 1207.3	9482	127.33	3.62:1

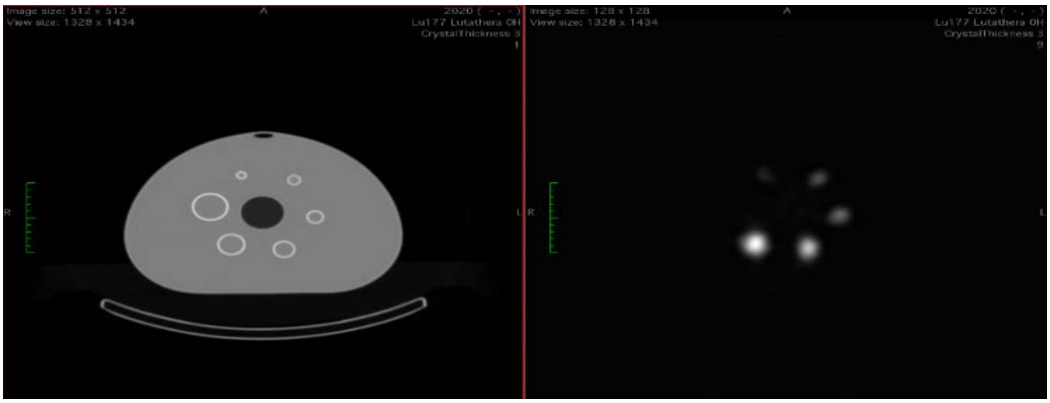

(a)

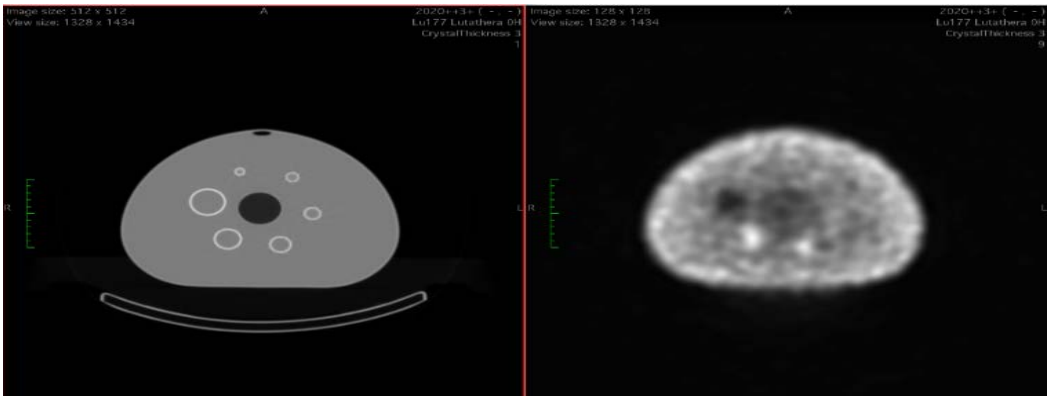

(b)

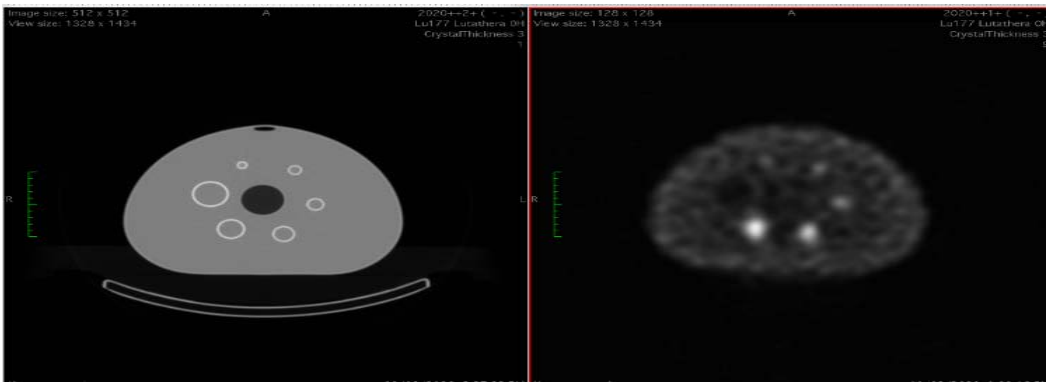

(c)

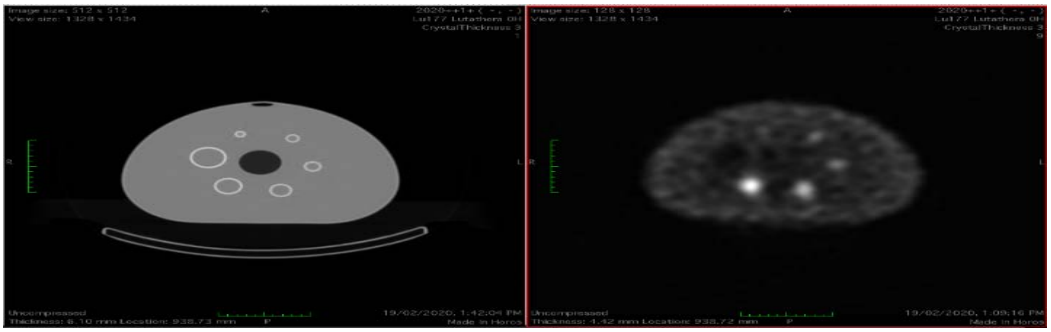

(d)

Figure 3. CT and SPECT image from NEMA image quality test for (a) no background; (b) 4:1; (c) 8:1 and (d) 16:1 hot sphere-to-background ratios.

2.2.1. Percent Contrast

The percent contrast was calculated by evaluation of various regions of interest in the transverse image slice that contained the centers of the spheres, as well as in adjacent slices as defined by NEMA standards. The percent contrast recovery Q was determined for each hot sphere as

$$Q = \frac{\left(C_{H,j}/C_{B,j}\right)-1}{\left(a_H/a_B\right)-1} * 100\% \tag{1}$$

where

$C_{H,j}$ = average counts in the ROI for sphere j;

$C_{B,j}$ = average of the background ROI counts for sphere j;

a_H = activity concentration in the hot spheres;

a_B = activity concentration in the background.

2.2.2. Background Variability

The percent background variability N_j for each sphere j, was given by Equation (2) below.

$$N_J = \frac{SD_J}{C_{B,J}} * 100\% \tag{2}$$

where SD_J is the standard deviation of the background ROI counts for sphere j, calculated as:

$$SD_J = \sqrt{\sum_{K=1}^{K}\left(\left(C_{B,j,K} - C_{B,j}\right)^2 / \left(k-1\right)\right)}, \tag{3}$$

where the sum is taken over the $K = 60$ background regions of interest.

2.2.3. Accuracy of Corrections

To measure the residual error using CT-based attenuation and scatter-corrected SPECT images, the relative error ($\Delta C_{lung,i}$) was calculated for each slice by calculating the ratio of the average counts in the lung insert ROI to the average counts in the background ROIs. The percentage of misplaced counts in the lung insert ($\Delta C_{lung,i}$) following the NEMA NU 2-2012 guidelines was defined by Equation (4) below. A circular ROI was drawn and centered on the lung insert and

the average pixel value within the ROI, C_{lung} for each image slice within the lung insert. The relative error C_{lung} was calculated for each slice and the residual error in the corrections was then measured using Equation (4).

$$\Delta C_{lung,i} = \frac{C_{lung,i}}{C_{B,37\,\mathrm{mm}}} \times 100\% \tag{4}$$

where $\Delta C_{lung,i}$ is the average counts in the lung insert ROI;

$C_{B,37\,\mathrm{mm}}$ is the of the average of the sixty 37 mm background ROIs.

3. Results and Discussion

3.1. NEMA Image Quality—Recovery Coefficients

The images obtained from the scans were imported from the Xeleris workstation onto the OXIRIS image analysis tool as shown in Figure 4. Regions of interest (ROIs) were drawn on each sphere of the reconstructed SPECT image, which was used for the analysis. ROIs of equal sizes were also drawn in the phantom background on the slice centered on the spheres. Twelve ROIs of diameter 36 mm were drawn in the background at a distance of 15 mm from the phantom edge. ROIs of the smaller sphere sizes (10, 13, 17, 22, 28 mm) were then drawn concentric to the 37 mm background ROIs. In all, a total of 60 background ROIs of each size and 12 ROIs on each of the five slices were drawn. The average counts in each background ROI were then recorded as shown in Table 2. ROIs placement for the hot spheres, cold sphere, lung insert and background is shown in Figure 5 below. The average background ROI counts for each hot sphere-to-background

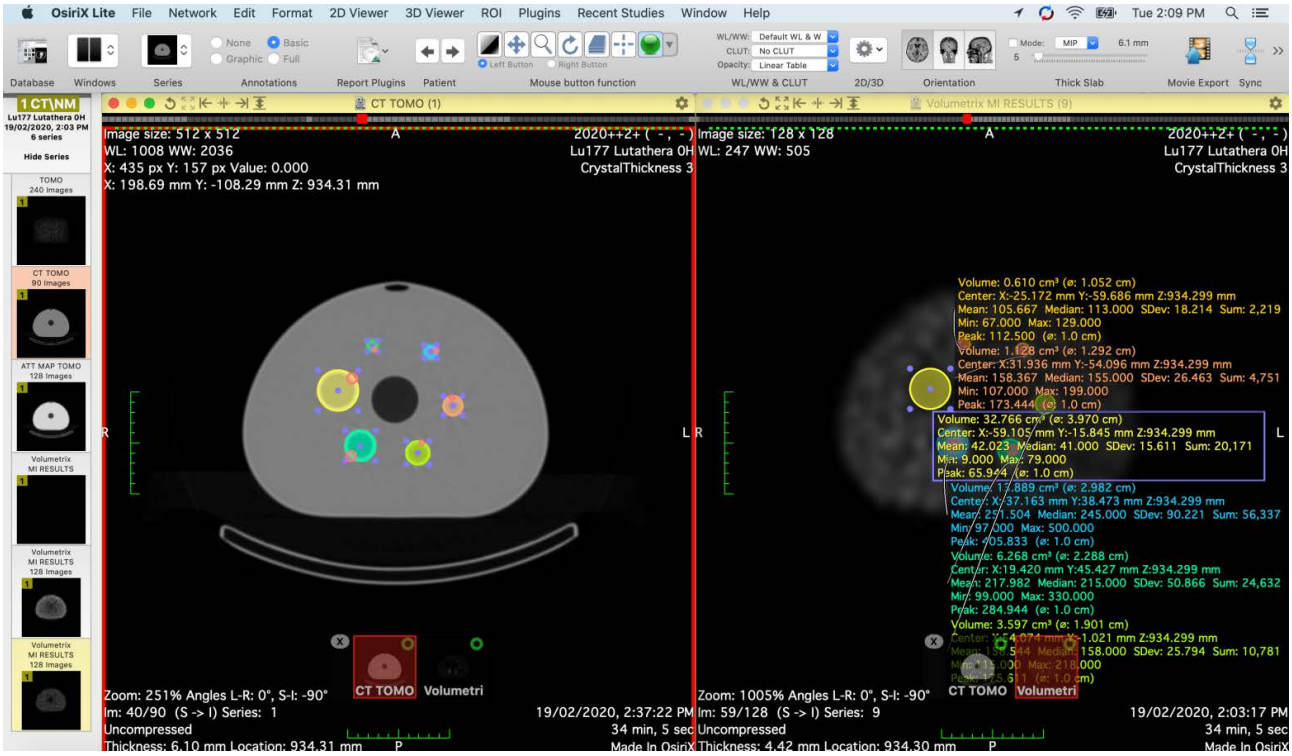

Figure 4. image imported onto Oxiris imaging tool for analysis showing regions of interest drawn on each sphere.

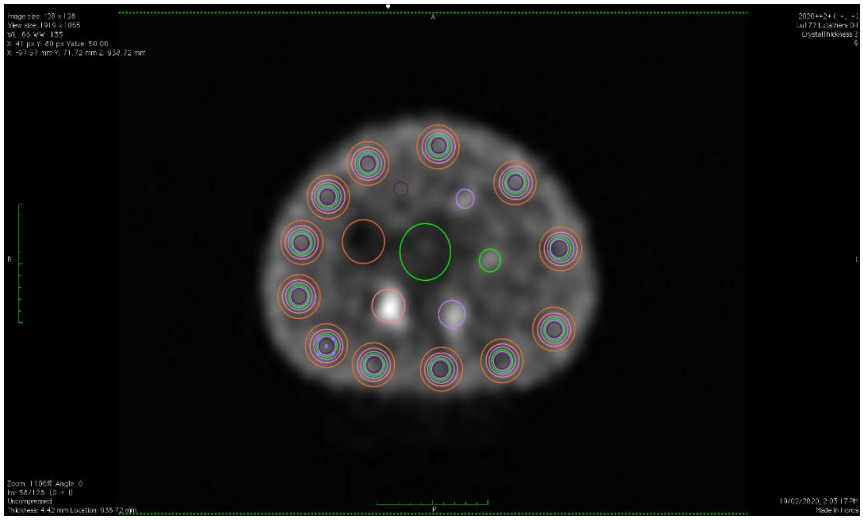

Figure 5. ROIs placement for hot spheres, cold sphere, lung insert and background. (ROIs of the smaller sphere sizes (10, 13, 17, 22, 28 mm) drawn concentric to the 37 mm background ROIs).

Table 2. Table showing the average ROI counts for the various spheres for each hot sphere-to-background ratio.

Average ROI counts for each sphere j, $C_{H,j}$	16:1	8:1	4:1	No background
Lung insert	1540.4	2000	4107.4	100.4
37 mm Cold Sphere	1217.4	1225	2753	9.8
28 mm hot sphere	7772.8	3186.6	4078	2678.6
22 mm hot sphere	4408.6	1778.4	2572.4	1426.8
17 mm hot sphere	2101.4	940.2	1575.8	557
13 mm hot sphere	1161.8	844.2	1234.2	332.6
10 mm hot sphere	551	376.6	739	112.8

Table 3. Table showing the average background ROI counts for each hot sphere-to-background ratio.

Average background ROI counts $C_{B,j}$ for:	37 mm Cold sphere	28 mm hot sphere	22 mm hot sphere	17 mm hot sphere	13 mm hot sphere	10 mm hot sphere
16:1	2314.916667	1078.416667	708.75	512.833333	233.8333	202.3333
8:1	3249.25	2105.833333	1426.66667	1075.58333	845.0833	603.5
4:1	6346.666667	4094.666667	2829.08333	1838.91667	1463.25	1017.417
No background	14.83333333	4.5000000	4.58333333	2.16666667	1.00000	0.916667

ratio was also recorded as shown in Table 3. The percent contrast, background variability and average lung residual error were calculated.

3.1.1. Percent Contrast

The image quality was analyzed by the contrast recovery according to the NEMA NU 2-2007 protocol. The 37 mm cold sphere had the highest percent contrast

whiles the 10 mm hot sphere had the least for the various hot sphere to background ratios. Table 4 gives the percent contrast for each sphere.

3.1.2. Background Variability

The percent background variability N_j, as a measure for the image noise for each sphere j, was determined and the results are shown in Table 5.

3.1.3. Accuracy of Corrections

The relative error C_{lung} was calculated for each slice and the residual error in the corrections was then measured. It was calculated to be 23.13% for the 16:1 and 22.57% for both the 8:1 and 4:1 hot sphere to background ratio Table 6 gives the average lung residual error.

Table 4. Table giving the percent contrast for each sphere.

Percent contrast Q for:	37 mm cold sphere	28 mm hot sphere	22 mm hot sphere	17 mm hot sphere	13 mm hot sphere	10 mm hot sphere
16:1	47.93%	43.8%	36.8%	21.9%	28%	12.2%
8:1	48.33%	53.33%	73.3%	69.5%	57.8%	35.9%
4:1	56.9%	55.55%	75.1%	70.5%	56.78%	32.78%

Table 5. Table giving the percent background variability for each sphere.

Percent Background variability for:	37 mm cold sphere	28 mm hot sphere	22 mm hot sphere	17 mm hot sphere	13 mm hot sphere	10 mm hot sphere
16:1	3.72	2.94	4.31	3.95	4.91	4.78
8:1	3.1	2.72	3.34	3.81	4.25	4.99
4:1	2.89	2.67	3.57	4.01	5.02	6.11

Table 6. Table showing the average lung residual error.

Hot sphere to background ratio	Average lung residual error %
16:1	23.12
8:1	22.57
4:1	22.57

4. Conclusion

In this work, a NEMA IEC body phantom was used which consisted of a body phantom, lung insert, and six spheres of various sizes. Image contrast and background variability ratios for hot spheres were used as measures of image quality. In addition, the accuracy of corrections was determined from the uniform background and cold lung insert regions. The study shows the percentage contrast increases with increasing sphere size. The results indicate that the scanner has very

good overall performance.

Conflicts of Interest

The authors declare no conflicts of interest regarding the publication of this paper.

References

[1] Ljunngberg, M., Celler, A., Konijnenberg, M.W., Eckerman, K.F., Dewaraja, Y.K. and Sjögreen-Gleisner, K. (2016) MIRD Pamphlet No. 26: Joint EANM/MIRD Guidelines for Quantitative ^{177}Lu SPECT Applied for Dosimetry of Radiopharmaceutical Therapy. *The Journal of Nuclear Medicine*, **57**, 151-162. https://doi.org/10.2967/jnumed.115.159012

[2] He, B. and Frey, E.C. (2006) Comparison of Conventional, Model-Based Quantitative Planar, and Quantitative SPECT Image Processing Methods for Organ Activity Estimation Using In-111 Agents. *Physics in Medicine and Biology*, **51**, 2967-3981. https://doi.org/10.1088/0031-9155/51/16/006

[3] Zhao, W., *et al.* (2018) Determination of Gamma Camera Calibration Factor for Quantification of Therapeutic Radioisotopes. *European Journal of Nuclear Medicine and Molecular Imaging Physics*, **5**, Article No. 8. https://doi.org/10.1186/s40658-018-0208-9

[4] Zaidi, H., Ojha, N., Morich, M., Griesmer, J., Hu, Z., Maniawski, P., *et al.* (2011) Design and Performance Evaluation of a Whole-Body Ingenuity TF PET-MRI System. *Physics in Medicine and Biology*, **56**, 3091-3106. https://doi.org/10.1088/0031-9155/56/10/013

[5] Delso, G., Fürst, S., Jakoby, B., Ladebeck, R., Ganter, C., Nekolla, S.G., *et al.* (2011) Performance Measurements of the Siemens mMR Integrated Whole-Body PET/MR Scanner. *The Journal of Nuclear Medicine*, **52**, 1914-1922. https://doi.org/10.2967/jnumed.111.092726

[6] Drzezga, A., Souvatzoglou, M., Eiber, M., Beer, A.J., Fürst, S., Martinez-Möller, A., *et al.* (2012) First Clinical Experience with Integrated Whole-Body PET/MR: Comparison to PET/CT in Patients with Oncologic Diagnoses. *The Journal of Nuclear Medicine*, **53**, 845-855. https://doi.org/10.2967/jnumed.111.098608

[7] Wiesmüller, M., Quick, H.H., Navalpakkam, B., Lell, M.M., Uder, M., Ritt, P., *et al.* (2013) Comparison of Lesion Detection and Quantitation of Tracer Uptake Between PET from a Simultaneously Acquiring Whole-Body PET/MR Hybrid Scanner and PET from PET/CT. *European Journal of Nuclear Medicine and Molecular Imaging*, **40**, 12-21. https://doi.org/10.1007/s00259-012-2249-y

[8] Paulus, D.H., Tellmann, L. and Quick, H.H. (2013) Towards Improved Hardware Component Attenuation Correction in PET/MR Hybrid Imaging. *Physics in Medicine and Biology*, **58**, 8021-8040. https://doi.org/10.1088/0031-9155/58/22/8021

[9] Kartmann, R., Paulus, D.H., Braun, H., Aklan, B., Ziegler, S., Navalpakkam, B.K., *et al.* (2013) Integrated PET/MR Imaging: Automatic Attenuation Correction of Flexible RF Coils. *Medical Physics*, **40**, Article ID: 082301. https://doi.org/10.1118/1.4812685

[10] Paulus, D.H., Thorwath, D., Schmidt, H. and Quick, H.H. (2014) Towards Integration of PET/MR Hybrid Imaging into Radiation Therapy Treatment Planning. *Medical Physics*. **41**, Article ID: 072505. https://doi.org/10.1118/1.4881317

[11] Oehmigen, M., Ziegler, S., Jakoby, B.W., Georgi, J.C., Paulus, D.H. and Quick, H.H.

(2014) Radiotracer Dose Reduction in Integrated PET/MR: Implications from National Electrical Manufacturers Association Phantom Studies. *The Journal of Nuclear Medicine*, **55**, 1361-1367. https://doi.org/10.2967/jnumed.114.139147

[12] Delso, G., Martinez-Möller, A., Bundschuh, R.A., Ladebeck, R., Candidus, Y., Faul, D. and Ziegler, S.I. (2010) Evaluation of the Attenuation Properties of MR Equipment for its Use in a Whole-Body PET/MR Scanner. *Physics in Medicine and Biology*, **55**, 4361-4374. https://doi.org/10.1088/0031-9155/55/15/011